Argonne NATIONAL LABORATORY

ANL/NSE-21/5

Validation and Demonstration of Control System Functional Capabilities within the IES Plug-and-Play Simulation Environment

IES Simulation Ecosystem Control System Development

Nuclear Science and Engineering Division

ANL/NSE-21/5

Validation and Demonstration of Control System Functional Capabilities within the IES Plug-and-Play Simulation Environment

IES Simulation Ecosystem Control System Development

prepared by
Haoyu Wang, Roberto Ponciroli, Richard B. Vilim
Nuclear Science and Engineering Division, Argonne National Laboratory
and
Andrea Alfonsi
Reactor Systems Design & Analysis Division, Idaho National Laboratory

January 31, 2021

Table of Contents

List of Figures

List of Tables

ABSTRACT

The concept of an integrated energy system (IES) is meant to combine different energy technologies in synergistic ways to achieve a more secure and economical energy supply. The RAVEN-based HYBRID framework is used to find the optimal installed capacity and the optimal economical dispatch of each component of the IES. The new RAVEN plugin for grid and capacity optimization (HERON) only addresses the limits that affect the production variables and the corresponding rates of variation (*explicit constraints*). However, other variables are subject to constraints, and the associated limits should be accounted for (*implicit constraints*). In particular, for the power dispatch problem, the optimization algorithm takes into account the limits on the electrical power output and the corresponding hourly power variations but does not consider other constraints on process variables whose response affects the service life of the IES.

This report describes a scheme that allows accounting for implicit constraints without increasing the size of the optimization problem. To obtain a more accurate approximation of the nonlinear dynamic behavior, a parametric version of the dynamic mode decomposition with control (DMDc) algorithm was developed to derive the state-space representation matrices of the IES components at different scheduling parameter. Thanks to this approach, a more accurate approximation of the system response can be obtained, the limits imposed by thermal mechanical implicit constraints can be translated into power dispatch limits, and the feedbacks to HERON power dispatcher can be provided.

To assess the developed methodology, a power dispatching test case composed of three power generating and storage units (Balance of Plant, Secondary Energy Source, Thermal Energy Storage) was developed. The power output of each one of the three units was optimized to meet the imposed time-dependent load demand trajectory and to maximize the IES profitability by meeting both the explicit and implicit constraints.

1. INTRODUCTION

In this work, the improvements to the reference governor (RG) algorithm that supports the power dispatch optimization scheme implemented in HERON [1][2] are described. To find a feasible solution to the power dispatch problem for the IES system, i.e., the optimization of the electrical power output by each one of the IES components, all the constraints affecting the flexible operation of the different IES components need to be accounted for. In addition to the limits that affect the instantaneous values of the production variables and the corresponding rate of variations (*explicit constraints*), there are other constraints that need be considered (*implicit constraints*) [3].

- *Electrical Power constraints (explicit constraints)*: the electrical power output can assume any value within a characteristic window, i.e., $P_{min} \leq P(t) \leq P_{max}$ (power limits). At the same time, electrical power variations cannot be too steep, i.e., $\left|\frac{dP}{dt}\right| \leq \left(\frac{dP}{dt}\right)_{max}$ (ramp-rate limits).
- *Thermo-mechanical constraints (implicit constraints)*: to avoid thermo-mechanical stress exceeding the design limits, temperature, pressure and flow rate need to be constrained as well, i.e., $T_{min} \leq T(t) \leq T_{max}$, $p_{min} \leq p(t) \leq p_{max}$, $w_{min} \leq w(t) \leq w_{max}$.

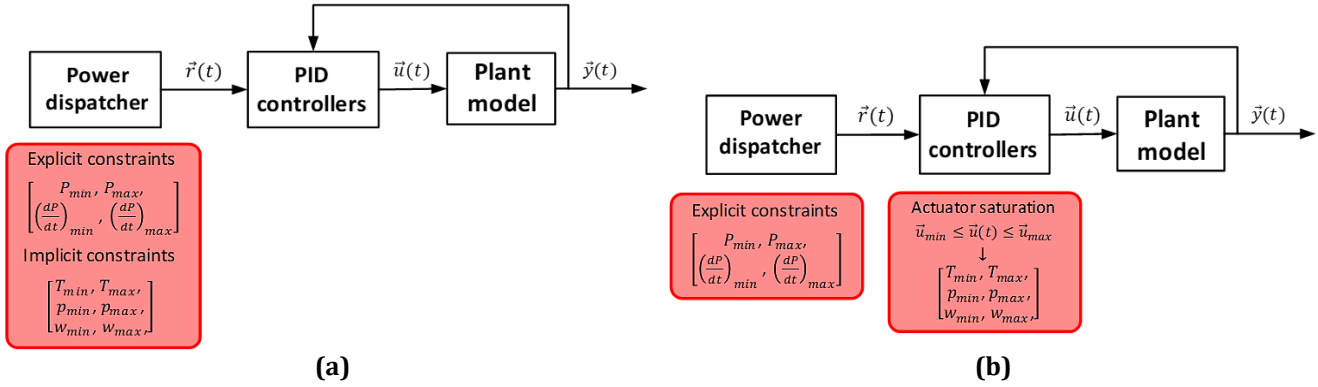

Figure 1-1. Tentative solutions to account for both explicit and implicit constraints into the optimization algorithm.

Ideally, all these constraints should be accounted for by the power dispatcher (Figure 1-1a). Unfortunately, the size of such optimization problem due to the simultaneous handling of all the single unit constraints would entail a large computational burden. The problem can be then addressed by splitting the set of constraints, i.e., the power dispatcher will take care of the explicit constraints, and the saturation limits on the PID controllers will take care of the implicit constraints (Figure 1-1b). This scheme is not suitable either, i.e., the final solution will be feasible and sub-optimal. Thanks to the imposed saturation limits of PID controllers, the set-points issued by the power dispatcher will generate control actions that will never cause the violation of any thermal mechanical constraints of the IES unit components, i.e., a feasible solution is granted. At the same time, the power dispatcher will account for only the explicit constraints (the size of the resulting

optimization problem will be manageable). As a result, the power dispatcher will provide optimal trajectories, but the saturation effects will limit the ensuing control actions in case they could cause the violation of the implicit constraints. The resulting power transients will then be sub-optimal, and the overall demanded power output will not be met.

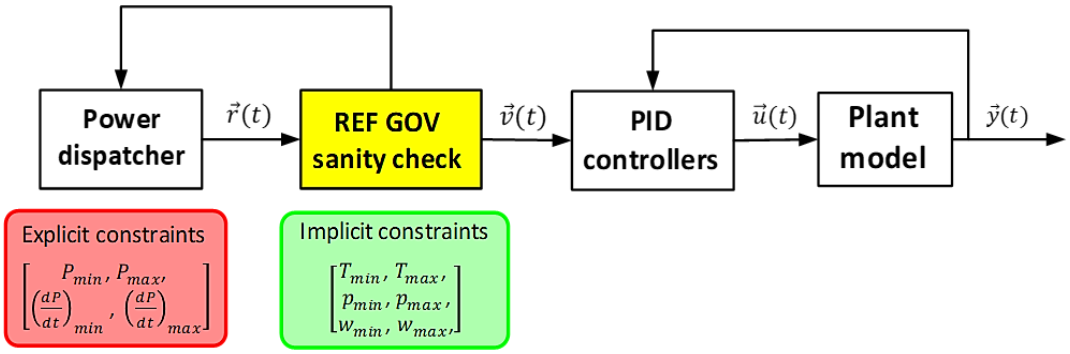

Figure 1-2. Proposed power dispatch scheme decoupling the explicit and the implicit constraints.

To overcome this problem, we proposed the insertion of the RG block into the optimization scheme (Figure 1-2). The power dispatcher will take care of the explicit constraints, and the RG algorithm will take care of the implicit constraints. When the tentative set-points are issued to the RG, the margins with respect to the bounds imposed by the implicit constraints will be evaluated and returned to the power dispatcher, which will re-optimize the power set-points during the following iteration. Thanks to this feedback configuration, the trajectories will be accepted only when the explicit constraint-compliant trajectories are "approved" by the RG block that behaves like a downstream sanity check.

2. TEST CASE

The developed test-case is constituted by a three-unit system, i.e., a gas turbine (secondary energy source, SES), a steam turbine (balance of plant, BOP), and a thermal energy storage facility (TES). An ideal constant source of high-quality steam is foreseen upstream to the BOP and to the TES. According to the results of the power dispatching, a portion of the steam will be devoted to the BOP (electrical power production), a portion to the TES (the produced heat will be stored), and the leftover will be discharged to the condenser. The BOP and the TES are thermally coupled (any pressure variation and flow rate variation due to BOP operation affects the TES operating conditions), whereas the SES is independent (Figure 2-1).

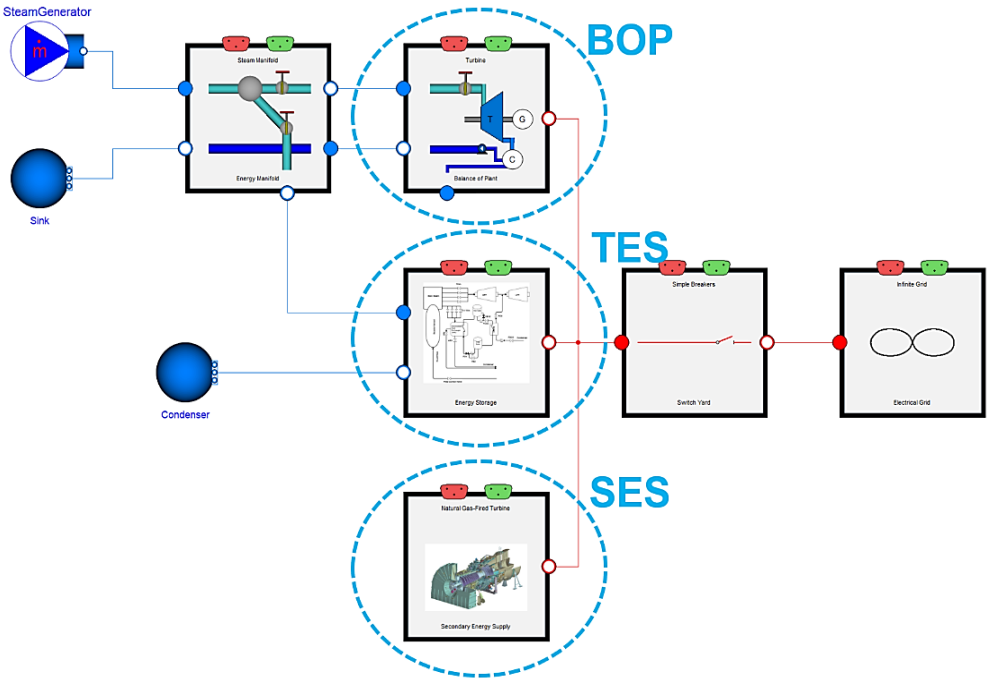

Figure 2-1. Graphical interface of the Dymola simulator representing the developed test-case.

With regard to the condenser, the currently adopted model is just a zero-dimensional sink that collects the steam flow rate that either is rejected by the BOP and by the TES or is discharged from the TES. The proposed optimization scheme foresees an RG for each on the IES units, i.e., the BOP, the SES, and the TES, but not for the condenser. In particular, the goal of the RG is to provide HERON with power-referred explicit constraints starting from the thermo-mechanical implicit constraints. Given the simplified model adopted to mimic its presence, there is no way to monitor the degradation or the damages of the condenser due to the occasional discharging of high-quality steam. For this reason, a surrogate model for this component will not be developed.

3. DERIVATION OF DATA-DRIVEN SURROGATE MODELS

3.1. Linear time-variant model

Since the RG algorithm is a model-based scheme, a simplified model of the system to be controlled will be needed to predict the future response and assess the feasibility of the input set-point trajectories. Given the nonlinear behavior of the IES components, the most convenient solution consists in adopting linear approximations derived from the Dymola simulations.

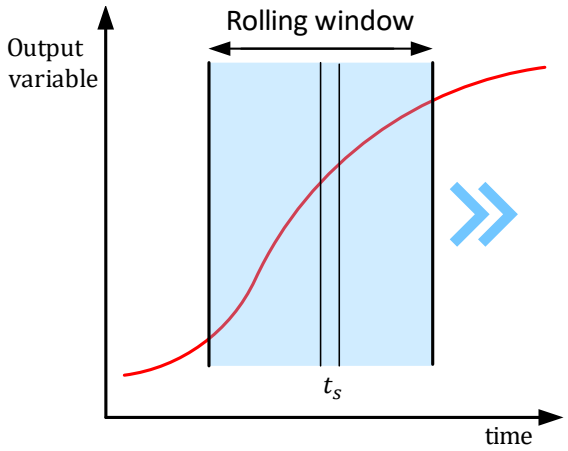

Figure 3-1. Graphical representation of the "rolling window" concept.

In particular, a rolling-window based approach (Figure 3-1) is envisioned, i.e., the evolution of the process variables within an hour would be used to derive the state-space representation matrices that will be adopted to predict the system response during the next hour. In this way, the state ($A(k)$) and the input ($B(k)$) matrices are updated at every time step (linear time-variant model, LTV).

$$x(k+1) = A(k)x(k) + B(k)u(k) \quad (1)$$

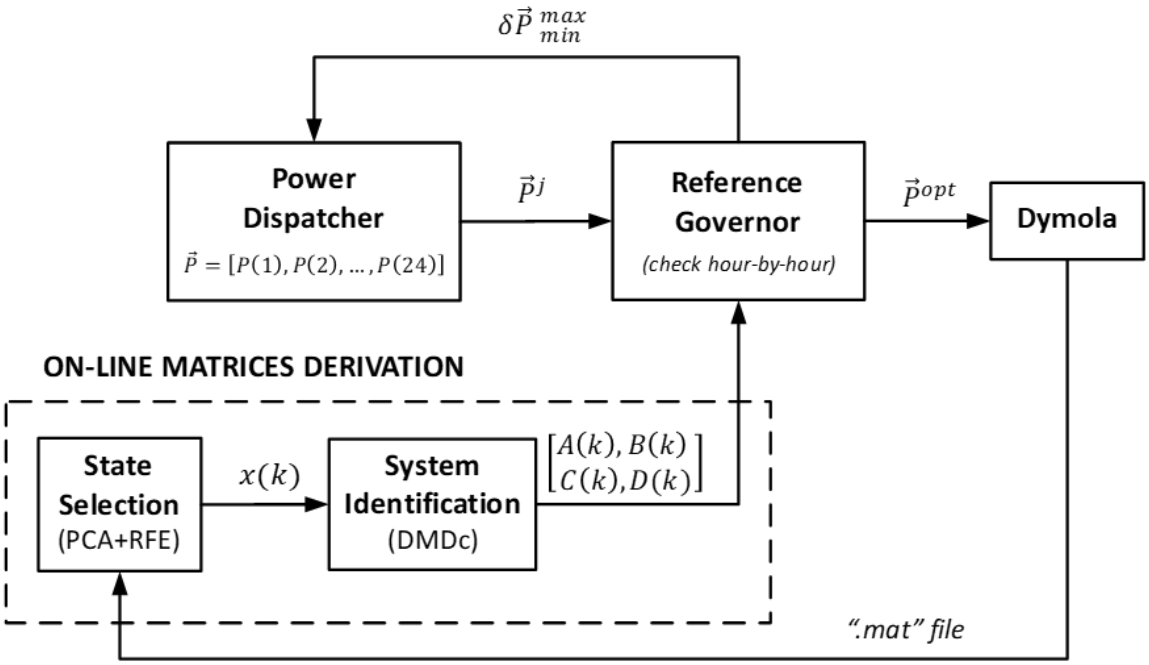

Figure 3-2. LTV model-based optimization scheme.

The drawback of this approach is that the high-fidelity, Dymola simulator of the overall system needs to be continuously run during the optimization process (Figure 3-2). That is not always the

case. When long term scenarios are studied, the computational burden due to the presence of the Dymola simulator might not be affordable. To perform this kind of analysis, a surrogate, parametrized model of the studied IES system is necessary. First, a set of Dymola simulation will be run off-line at different power levels. The evolution of the main process variables during the simulated power transients will be collected. By applying the DMDc algorithm, state-space representation matrices will be derived for each operating condition, i.e., a database of state-space matrices indexed by setpoint levels will be built. This database will be used during the RG-based optimization process. When the solution of the power dispatch is found, the validation will be performed by adopting the rolling-window based scheme.

3.2. Linear parameter-varying model

A linear parameter-varying (LPV) system is a linear state-space model whose dynamics vary as function of certain time-dependent parameters called *scheduling parameters* [4][5]. Mathematically, a LPV system is represented as

$$x(k+1) = A(p)x(k) + B(p)u(k) \tag{2}$$

$$y(k) = C(p)x(k) + D(p)u(k) \tag{3}$$

where $A(p)$, $B(p)$, $C(p)$ and $D(p)$ are the state-space matrices parametrized by the scheduling parameter vector (p). The parameters $p(t)$ are measurable functions of the inputs and the states of the system. They can be a scalar quantity or a vector of several parameters. The set of scheduling parameters define the *scheduling space* over which the LPV model is defined.

A certain number of anchor points in the *scheduling space* are selected. The LPV system is constituted by a set of linear time invariant (LTI) models for the plant to be controlled that are obtained by linearizing around each anchor points in the *scheduling space*. These LTI models will be used to represent the dynamics in the local vicinity of that anchor point. Thanks to these multiple approximations, the LPV model provides the approximation of the behavior over a span on operating conditions (Figure 3-3).

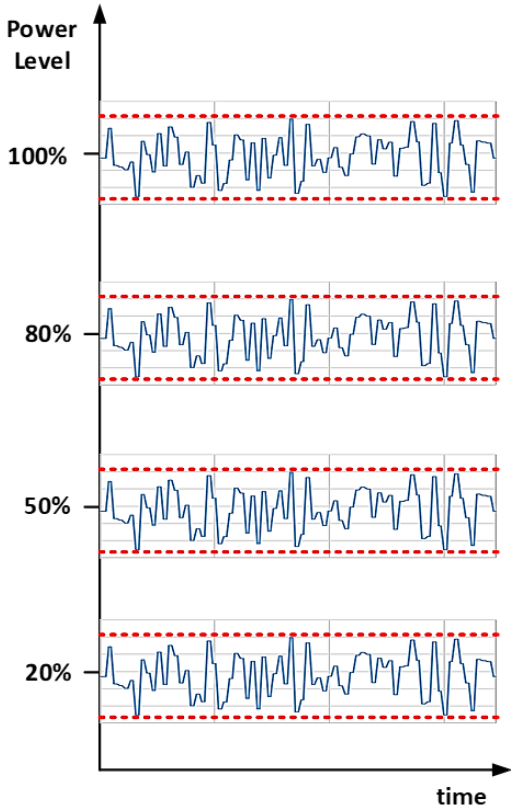

Figure 3-3. Imposed perturbations at different power levels. The system responses evaluated in the proximity of the selected points in the scheduling space are used to derive the single LTI models.

3.3. Implementation of the LPV model in the Optimization scheme

The goal is to derive a LPV model for each one of the units that constitute the developed test-case, i.e., the SES, the BOP, and the TES. With respect to the operating range of a single IES component, a certain number of operating conditions are identified. The idea is that a LTI model of each studied system will be derived around these operating conditions. To this aim, small amplitude transients will be simulated, the results will be collected, and the corresponding LTI models will be derived by applying the DMDc algorithm. The sets of state-space representation matrices corresponding to the studied operating conditions will then be labelled according to the values assumed by the scheduling parameters. In this way, the LPV model will be obtained. This operation will be repeated for all the IES components. The LPV models will be then used in the RG algorithm, as shown in Figure 1-2.

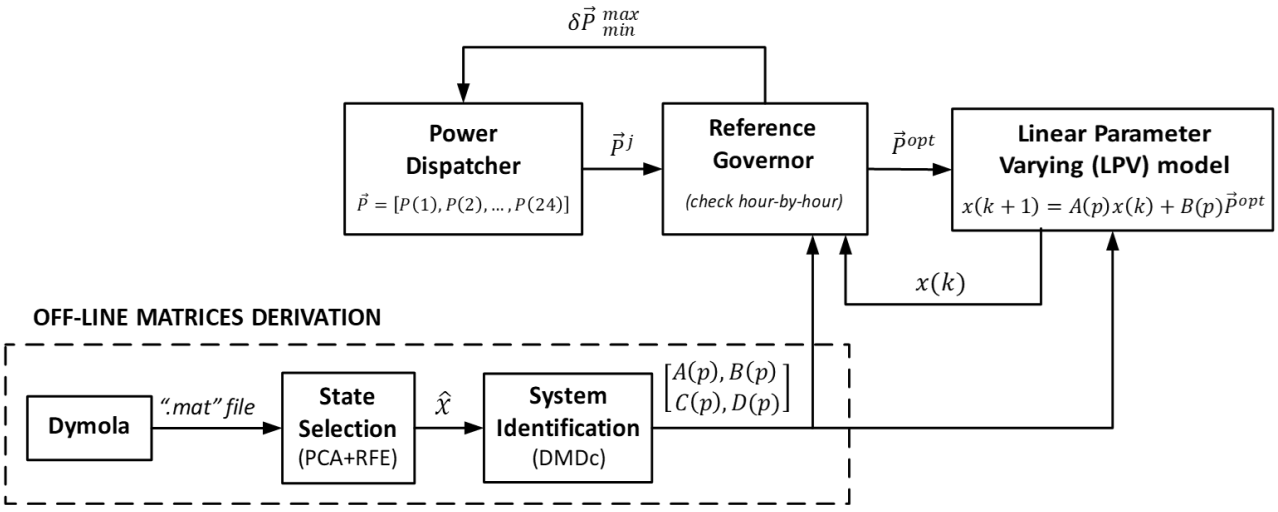

Figure 3-4. LPV model-based optimization scheme.

3.4. Tracking of the state variable evolution

The constraints affecting the operation of the TES have a peculiarity with respect to the constraints limiting the BOP and the SES power transients, i.e., the permitted range of the power set-point ($\vec{P}^{opt}$) for the TES is affected by the current values of the state variables ($\vec{x}(k)$). As discussed in [3], at the beginning of k^{th} hour, the RG validator needs the state vector to predict the system response ensuing from the application of the power set-point (Figure 3-4). For the optimization of the BOP and the SES power outputs, a constant zero vector can be fed to the RG at the beginning of every hour. Once the power set-point is issued, the BOP and the SES can reach the corresponding steady-state conditions in a relatively short time regardless of the initial value of system state vector. On the other hand, the state vector of the TES contains information about the instantaneous charging level. If the RG validator have no access to the accurate information of current charging level, the safety operational margin might shrink, resulting in over-charging or over-discharging to the installed TES device. To address this issue, the state vector needs to be projected in time along with the optimized power set-point to reflect the charging/discharging effect and track the TES power history (Eq.(2)). The RG validator will need to be provided with the updated system state vector at the beginning of the next hour to evaluate the current charging level and calculate the permitted operational margin.

4. REFERENCE GOVERNOR VS COMMAND GOVERNOR

Since the studied test case is constituted by multiple units, the suitable algorithm for the supervision of large-scale networked systems requiring constraints fulfillment would be the distributed command governor (CG) [6]. A CG is a non-linear device that outputs a reference trajectory rather than a control input and that it is imposed to a primal compensated control system. Whenever necessary, the CG modifies the reference signals supplied to the primal control system to avoid constraint violations. One of the advantages of CG usage lies in its simplicity in addressing

constrained tracking problems. The CG strategy seems to be very suitable in the supervision of large-scale networked systems where constraints fulfillment is a crucial task. The distributed CG represents a parallel distributed approach that allows computing set-point signals that are compliant with the single component constraints while ensuring global constraints satisfaction.
With respect to the proposed application of the RG/CG into the power dispatch optimization algorithm, the capability of meeting global constraints is not necessary. In case the respect of the local constraints would lead to the violation of a global constraint, the CG would provide some sort of compensation. This contribution would turn out to be expendable. The calculated limits would be returned to HERON and a new optimization would be performed, and a new set of set-point signals would be generated anyway.
Therefore, given the feedback configuration of HERON and the RG blocks, the capability of handling global constraints and providing mutual compensation are not required. To this aim, a set of local RG components would be sufficient. The role of the RG consists in (1) evaluating the margins of the normal operation envelope for each one of the IES components, (2) converting these limits into suitable constraints for the imposed power set-points. All the decision-making capabilities are embedded into HERON optimization algorithm.
In addition, the adopting of the distributed CG would have required a more sophisticated state-space representation model of the system network. Let us consider a set of n sub-systems, each one being a LTI closed-loop dynamical system regulated by a local controller which ensures stability and good closed-loop properties within linear regimes (when the constraints are not active). Let the i^{th} closed-loop subsystem be described by the following discrete-time model [6]:

$$x_i(k+1) = A_{ii}x_i(k) + B_i g_i(k) + \sum_{j \in n-\{i\}} A_{ij}x_j(k) \tag{4}$$

$$y_i(k) = C_i x_i(k) \tag{5}$$

where $k \in \mathbb{Z}^+$, x_i is the state vector (which includes the controller states under dynamic regulation), g_i is the manipulable reference vector which, if no constraints (and no CG) were present, would coincide with the set-points issued by HERON.
A_{ii} matrices represent the impact that the current values of the i^{th} component state variables (x_i) will have on their own future response. A_{ij} matrices represent the impact that the current values of the j^{th} component state variables (x_j) will have on the future response of x_i variables. To derive the LTI models that constitute the LPV model of each component, the DMDc algorithm is used. To estimate A_{ij} matrices (off-diagonal contributions), a modified version of the algorithm would need to be developed.

4.1. Modification of the RG algorithm

Each one of the IES unit components will be modeled as a Single Input Multiple Output system. The corresponding models receives as input the adjusted set-point trajectory (v), and returns as outputs the monitored process variables ($\vec{y}$). The detailed description of the RG algorithm is reported in [3]. With regard to the developed test-case, the version of the RG algorithm needed to be adjusted when it was applied to the TES model. In particular, the set of linear inequalities to be met during both steady-state and transient conditions was modified. Let us consider a system characterized by p output variables ($\vec{y} = [y_1, y_2, \dots, y_p]^T$), and let us impose a lower and an upper limit to each one of these variables. These bounds can be represented by a set of linear inequalities, i.e., $y_1 \geq {y_1}^{min}$ and $y_1 \leq {y_1}^{max}$. For simplicity, let us assume that these constraints are constant (Eq.(6)).

$$\begin{bmatrix} +1 & 0 & \cdots & 0 \\ -1 & 0 & \cdots & 0 \\ 0 & +1 & \cdots & 0 \\ 0 & -1 & \cdots & 0 \\ \vdots & \vdots & \ddots & \vdots \\ \vdots & \vdots & \ddots & \vdots \\ 0 & 0 & \cdots & +1 \\ 0 & 0 & \cdots & -1 \end{bmatrix} \cdot \begin{bmatrix} y_1 \\ y_2 \\ \vdots \\ y_p \end{bmatrix} \leq \begin{bmatrix} +{y_1}^{max} \\ -{y_1}^{min} \\ +{y_2}^{max} \\ -{y_2}^{min} \\ \vdots \\ +{y_p}^{max} \\ -{y_p}^{min} \end{bmatrix} \Rightarrow S \cdot \vec{y} \leq \vec{s} \tag{6}$$

When constant input signals are supplied ($v(k) = v$), the state variables usually do not change at steady state ($\vec{x}(k) = \vec{x}$). Let us define the matrix T as the ratio between the state of the system and the corresponding inputs (Eqs.(7)(8)).

$$\vec{x} = A^d \cdot \vec{x} + B^d \cdot v \tag{7}$$

$$T = \frac{\vec{x}}{v} = (I - A^d)^{-1} \cdot B^d \tag{8}$$

By adopting Eq.(5) and Eq.(8), the linear inequalities in Eq.(6) can be rewritten at steady state as follows:

$$S \cdot \vec{y} = SC^d T v + SD^d v \leq \vec{s} \tag{9}$$

In the traditional formulation of the RG algorithm, the inequality reported in Eq.(9), which enforce the respect of the limits at the end of the transient, is added to the other ones. In case the RG is applied to a TES system, this inequality needs to be dropped. During the charging phase, the TES behaves like an integrator, i.e., it keeps accumulating the thermal energy that is diverted from the BOP. If the power set-point is constant, a constant steam flow rate keeps flowing through it, and the amount of stored energy keep increasing. For this kind of systems, the application of a constant non-zero input signal will not lead the system to reach steady-state conditions.

Symmetrically, the same behavior can be observed during the discharging phase, i.e., the TES system will never reach steady-state conditions if constant input signals are supplied.

A second consequence of this feature of the TES system is that the corresponding prediction horizon needs to be set to cover the adopted time interval of the power dispatch optimization process. In the current formulation of the power dispatch problem, the power set-points are adjusted on hourly basis. With regard to the TES operation, this means that the incoming steam flow rate is imposed at the beginning of the hour, and it is not changed till the very end of the hour. Since the value of the incoming steam flow rate is constant throughout the current hour and the inequality reported in Eq.(9) had to be dropped, the prediction horizon to ensure the respect of the maximum storage capacity constraint needs to be one-hour long.

5. DMDC AS AN EXTENSION OF EXISTING DMD ALGORITHM

As previously mentioned, the RG algorithm requires the identification of the state-space representation matrices *A* and *B* to predict the system response ensuing from the performed control actions. To get the needed matrices, a system identification technique, i.e., the dynamic mode decomposition with control (DMDc) [7], was used. The DMDc is an extension of the dynamic mode decomposition (DMD) method, which was firstly developed by Schmid in 2008 [8] and expanded by different scientists for improved accuracy and performance, e.g., multi-resolution, high-order, etc. Given a realization (time series of data), the DMD algorithm can be used to compute a set of modes each of which is associated with a fixed oscillation frequency and decay/growth rate. The DMDc allows distinguishing between the underlying dynamics and the influence of the system inputs, resulting in accurate input-output models, i.e., DMDc algorithm allows obtaining the A^d and B^d state-space representation matrices of the monitored system dynamics. Since the derived matrices represent the best-fit solutions for the data contained in the training set, the relationship in Eq.(10) does not hold exactly:

$$\vec{x}(k+1) \approx A^d \vec{x}(k) + B^d \vec{v}(k) \tag{10}$$

The matrices can be constructed by collecting temporal snapshots (time samples) of the system states and inputs over time (Eq.(11)).

$$\begin{aligned} \mathrm{X}' &= \begin{bmatrix} | & | & & | \\ x(2) & x(3) & \cdots & x(l) \\ | & | & & | \end{bmatrix} \\ \mathrm{X} &= \begin{bmatrix} | & | & & | \\ x(1) & x(2) & \cdots & x(l-1) \\ | & | & & | \end{bmatrix} \\ \mathrm{U} &= \begin{bmatrix} | & | & & | \\ v(1) & v(2) & \cdots & v(l-1) \\ | & | & & | \end{bmatrix} \end{aligned} \tag{11}$$

where each column represents either the state ($\vec{x}(k)$) or the input arrays ($\vec{v}(k)$) evaluated at a certain time step. Eq.(10) can be rewritten in a matrix form to include the new data matrices:

$$\mathrm{X}' \approx A^d \mathrm{X} + B^d \mathrm{U} \tag{12}$$

Since there are two unknown matrices A^d and B^din the equation, Eq.(12) can be rewritten as

$$\mathrm{X}' \approx G\Omega \tag{13}$$

where $G = [A^d, B^d]$ and $\Omega = [X, U]^T$. Thus, the operator $G \in \mathbb{R}^{n\times(n+m)}$ can be calculated as

$$G = \mathrm{X}'\Omega^{\dagger} \tag{14}$$

To solve Eq.(14), the singular value decomposition (SVD) is applied to the augmented data matrix Ω, which leads to:

$$\Omega = \mathrm{U}\Sigma\mathrm{V}^* \approx \tilde{\mathrm{U}}\tilde{\Sigma}\tilde{\mathrm{V}}^* \tag{15}$$

where $\tilde{\mathrm{U}} \in \mathbb{R}^{(n+m)\times q}$, $\tilde{\Sigma} \in \mathbb{R}^{q\times q}$, and $\tilde{\mathrm{V}} \in \mathbb{R}^{(l-1)\times q}$ are the truncated SVD components. The truncation value q is the number of non-zero elements in Σ by default, but it can be manually defined to a smaller value if desired. Eq.(16) provides an approximation of G

$$G \approx \bar{G} = \mathrm{X}'\tilde{\mathrm{V}}\tilde{\Sigma}^{-1}\tilde{\mathrm{U}}^* \tag{16}$$

By breaking the linear operator $\tilde{\mathrm{U}}$ into two separate components according to the dimensions of $\vec{x}(k)$ and $\vec{v}(k)$, the approximations of the matrices A^d and B^d can be found (Eq.(17)).

$$[A^d \quad B^d] \approx [\mathrm{X}'\tilde{\mathrm{V}}\tilde{\Sigma}^{-1}\tilde{\mathrm{U}}_1^* \quad \mathrm{X}'\tilde{\mathrm{V}}\tilde{\Sigma}^{-1}\tilde{\mathrm{U}}_2^*] \tag{17}$$

where $\tilde{\mathrm{U}}_1 \in \mathbb{R}^{n\times q}$ and $\tilde{\mathrm{U}}_2 \in \mathbb{R}^{m\times q}$. The algorithm here reported has been deployed in the RAVEN framework, as augmentation of the DMD base method already available.

6. PARAMETRICAL DMDC

In previous section, the main steps of the DMDc algorithm were presented. The DMDc-derived matrices approximate the system dynamics around the operational conditions of the realization (time series) that was used. Since the models fed to the RG are expected to represent the system response over a wide range of operating conditions, an augmented approach was derived. A method, called parametric dynamic mode decomposition with control (PDMDc) for allowing the DMDc-base method to capture the distortion of the underlying matrices in case of operational condition deviations was developed.

The basic idea behind the PDMDc algorithm is to segment the operational condition domain into multiple sub-domains, characterized by specific coordinates in the phase space (e.g., power levels). For each coordinate in the phase space (parameters), the governing system matrices A and B are evaluated via the DMDc method explained in the previous section, resulting in a set of matrices that are now dependent on the scheduling parameter (p),

$$[A^d(p) \quad B^d(p)]$$

The segmentation of the operational domain is performed employing perturbations of the operational conditions via one of the RAVEN forward sampling techniques. The resulting multiple realizations of the dynamic system are then processed by the PDMDc for the construction of the parametrized model.

6.1. Development of a dedicated procedure for state variable selection

In the evaluation of the multiple LTI models that constitute the LPV model, originally, the state variables were independently selected. An issue came up during the evaluation of the TES model. Given the non-linear dynamic features, the number of selected variables depended on the power levels. The number and the type of the state variables need to be the preserved at different operating conditions. The state-space representation model will refer to these variables and will project the value of these state variables in the future. If the number and the type of these variables change, the predictions will not be consistent and the initialization will not be possible, i.e., the power history of the component could not be tracked (Figure 6-1). To address this issue, a dedicated methodology was developed. This method is based on the deployment of cascade of data projection/processing consisting in (1) the feature space dimensionality reduction and projection in the reduced space, and (2) the feature selection step in the reduced space.

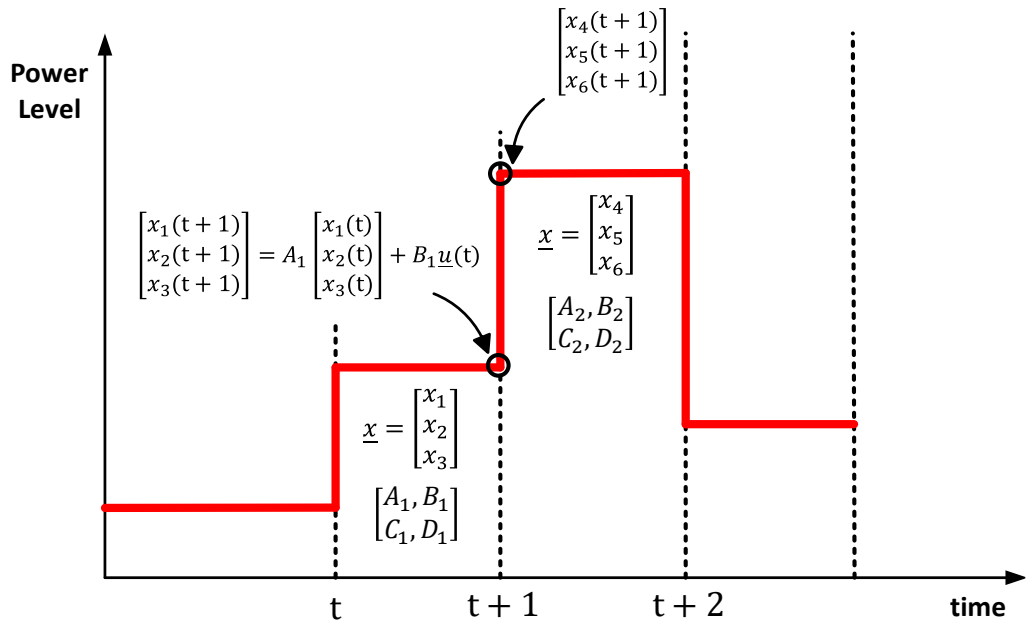

Figure 6-1. Initialization issue that might ensue from independent derivations of LTI models.

6.2. Feature dimensionality reduction via principal component analysis

To lessen the risk of model overfitting and to reduce the number of state-variables that are considered in the characterization of the system, the feature space (number of state-variables) must be reduced. To achieve this goal with a consistent and robust approach, the principal component analysis (PCA) method was applied. The PCA is a technique for reducing the dimensionality of large, high-dimensional datasets (with n observations on p numerical variables), increasing interpretability but at the same time minimizing information loss. The approach achieves it creating new uncorrelated variables/dimensions (principal components) that maximize the variance within the dataset. The method basically consists in solving an eigenvalue/eigenvector problem. Formally, the data values define a data matrix $X \in \mathbb{R}^{n \times p}$, whose j^{th} column is the vector $\vec{x}_j$ of observations on the j^{th} variable. As mentioned herein, the PCA method seeks a linear combination of the columns of matrix X with maximum variance. Such linear combinations are given by

$$\sum_{j=1}^{p} a_j \vec{x}_j = X\vec{a} \tag{18}$$

where $\vec{a}$ is a vector of constants $a_1, a_2, \ldots, a_p$. The variance of any linear combination is given by

$$var(X\vec{a}) = \vec{a}^T S \vec{a} \tag{19}$$

where S is the sample covariance matrix associated with the dataset.
Hence, identifying the linear combination with maximum variance is equivalent to obtaining a *p-dimensional* vector $\vec{a}$ which maximizes the quadratic form $\vec{a}^T S\vec{a}$. To produce a defined solution to the problem, a constraint needs to be imposed; commonly, the restriction involves the requirement to work with unit-norm vectors ($\vec{a}^T\vec{a} = 1$). Consequentially, the problem is equivalent to the optimization of $\vec{a}^T S\vec{a} - \lambda(\vec{a}^T\vec{a} - 1)$, where λ is a Lagrange multiplier. Differentiating with respect to the vector $\vec{a}$ and equating to the null vector, produces the equation

$$S\vec{a} = \lambda\vec{a} \tag{20}$$

Thus, $\vec{a}$ must be a (unit-norm) eigenvector, and λ the corresponding eigenvalue, of the covariance matrix S. Any real symmetric matrix $\in \mathbb{R}^{p\times p}$, such as a covariance matrix S, has exactly p real eigenvalues λ_k ($k = 1, \dots, p$), and their corresponding eigenvectors can be defined to form an orthonormal set of vectors

$$\begin{cases} \vec{a}_k{}^T\vec{a}_{k'} = 1 & if\ k = k' \\ 0 & if\ k \neq k' \end{cases} \tag{21}$$

The main idea using this approach in this project is to reduce the dimensionality of the feature space still capturing the main drivers in the feature dataset. The PCA method is applied on the feature space only (no output variables) for the construction of a new reduced dataset. To overcome the issue reported in Section 6.1, both the state variable space and the parameter space [X p] are processed together in the PCA process, resulting in a set of principal components that capture the both the system dynamic drivers and the parameter perturbations.

6.3. Feature dimensionality reduction via recursive feature elimination

Besides the application of the PCA to the state-variable and parameter spaces, a further reduction of the computational cost and risk for overfitting in terms of model output can be obtained by applying an algorithm for feature selection. At this stage of the process, the features, on which the feature selection process is applied, are represented by the principal components (transformed space) only. To this aim, feature-ranking techniques are particularly attractive since they allow selecting a fixed number of top ranked features for construction of representative models and/or identification of important dimensions/inputs for the figure of merits of interest. Among the available approaches, the recursive feature elimination (RFE) and its variant cross-validated recursive feature elimination (CVRFE) were deployed in the RAVEN framework. The method consists of the following iterative procedure:

1. Construct an evaluation model, trained on a complete feature space dataset.
2. Compute a *ranking criterion* for all features by using:

2.1. Sensitivity ranking method (ranking of the features based on their sensitivity coefficients)
2.2. Correlation ranking approach (ranking of the features based on their correlation coefficients)
3. Remove the feature with smallest ranking criterion.

This iterative procedure is an instance of backward feature elimination. For computational reasons, it may be more efficient to remove several features at a time, at the expense of possible classification performance degradation. In such a case, the method produces a feature subset ranking, as opposed to a feature ranking. Feature subsets are nested $F_1 \subset F_2 \subset F_3 \ldots \subset F$. If features are removed one at a time, there is also a corresponding feature ranking. However, the features that are top ranked (eliminated last) are not necessarily the ones that are individually most relevant. Only taken together the features of a subset $\vec{F}_m$ are optimal in some sense. At the end of this process, a set of principal components that are drivers in the system dynamic are selected. These principal components represent the feature space of the DMDc algorithm.

7. IES COMPONENTS SURROGATE MODELS

7.1. SES model

In Figure 7-1, the current configuration of the SES component is shown. A detailed view of the graphical user interface is shown to the right. Two dedicated system buses are implemented, i.e., the "sensorBus" and the "actuatorBus". The former collects the process variables whose evolution needs to be controlled (output variables, red dashed trajectories). The latter collects the signals that are sent to the system actuators (green dashed trajectories). The control scheme governing the evolution of the plant model is contained in the block labelled "Control" at the top of this picture. It is a PID controller that generates a signal controlling the gas flow rate, based on the demanded power and sent back to the system through the "actuatorBus".
The SES thermo-mechanical constraints are discussed in [3]. As a quick summary, the electrical power output is limited within 13.5MW and 50MW, and the gas turbine firing temperature is limited within 816℃ and 1600℃ to avoid carbon monoxide production or turbine mechanical structure damage.

SES scheduling parameter

To label and identify the set of state-space representation matrices approximating the SES operating conditions, suitable parameters are needed. In this simple feedback control scheme, the controller will increase/decrease the gas flow rate proportionally to the electric power demand. To this aim, the state-space representation matrices can be parametrized with respect to the value of the gas flow rate, and in turn to the instantaneous demanded electric power level.

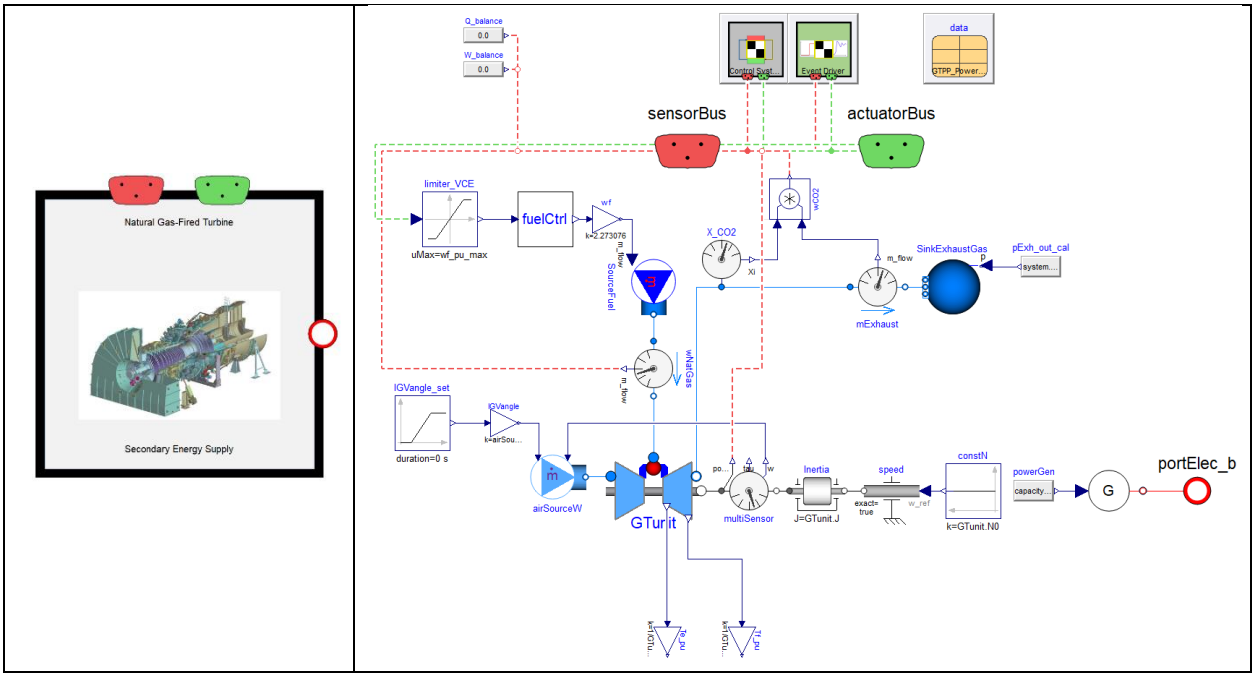

Figure 7-1. Graphical interface of the Dymola SES model (left), detailed view (right).

7.2. BOP model

The current configuration of the BOP component is shown in Figure 7-2. A detailed view of the graphical user interface is shown to the right. Being similar to the SES model mentioned in Section 7.1, the process variables to be monitored (inlet steam pressure, generated electric power) are returned to the PID controller through the "sensorBus", and the actuation signal controlling the opening of turbine control valve "valve_TCV" and bypass valve "valve_BV" are fed into the system through "actuatorBus". As seen in Figure 7-2, the inlet steam flow from "port_a" is split into two parts, i.e., a portion is fed into the steam turbine through the turbine control valve "valve_TCV" for electric power generation and then discharged to the condenser, while the other portion is fed to the condenser directly through the bypass valve "valve_BV". The condensed water is then fed to the reservoir of the feed water heater and exit through "port_b" after being heated by the external steam from "port_a3".

The BOP thermo-mechanical constraints are discussed in [3]. The electrical power output is limited within 725MW and 1450MW, and the steam turbine inlet pressure is constrained to 2 bar operational variation to avoid mechanical degradation within the steam turbine.

BOP scheduling parameter

In this feedback control scheme, the controller will increase the turbine control valve opening and decrease the bypass valve opening when a higher electric power is demanded, thus directs more steam flow to the steam turbine for electricity production. The turbine control valve opening will be reduced and more steam will be directed to the bypass route at a lower demanded electric

power. To this aim, the state-space representation matrices can be parametrized with respect to the openings of the two valves, and in turn to the instantaneous demanded electric power level.

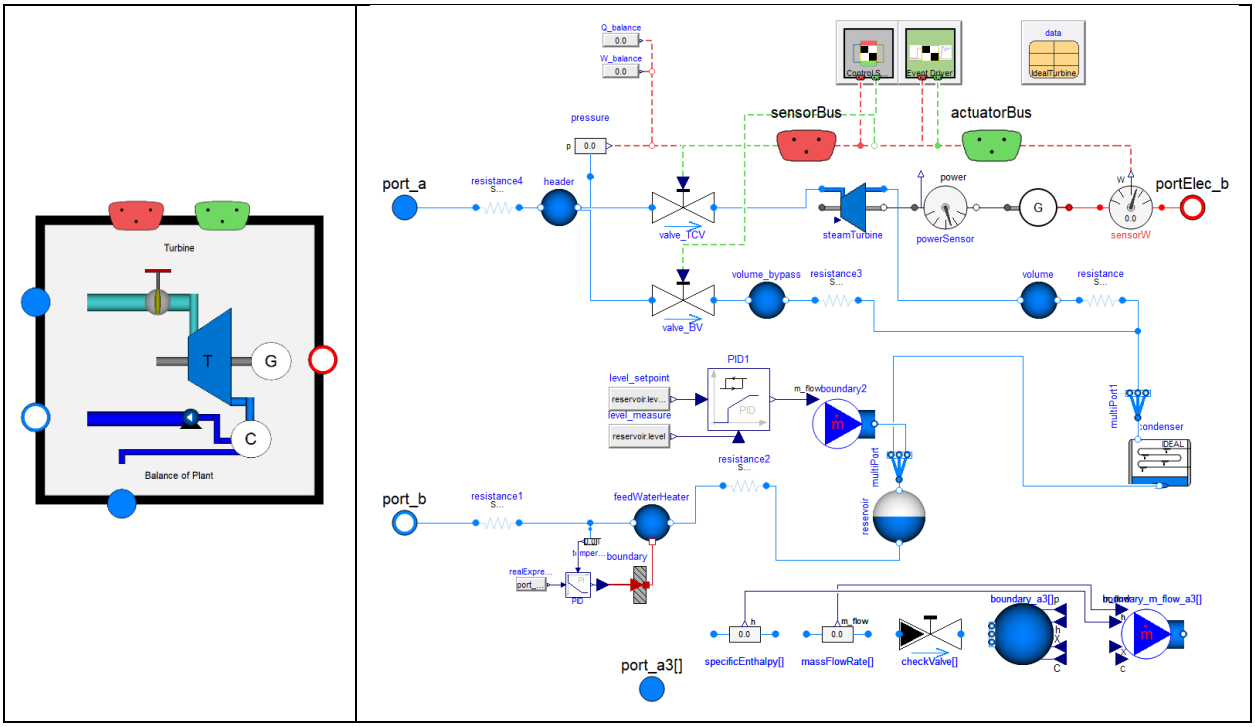

Figure 7-2. Graphical interface of the Dymola BOP model (left), detailed view (right).

7.3. TES model

In Figure 7-3, the configuration of the TES system that is coupled with the BOP is represented. The hydraulic loop consists of two large storage tanks along with pumps to transport the TES fluid between the tanks, the intermediate heat exchanger (IHX), and a steam generator. During low-demand periods, a portion of the steam flow rate is directed to the TES unit through the auxiliary bypass valves where it condenses on the shell side of the IHX. TES fluid is pumped from the cold tank to the hot tank through the tube side of the IHX at a rate sufficient to raise the temperature of the TES fluid to some set-point. The TES fluid is then stored in the hot tank at constant temperature. Condensate is collected in a hot well below the IHX and drains back to the main condenser.

"Charging" mode

During charging mode operation, the IHX exit temperature on the inner loop and the level in the IHX are controlled by adjusting the FCV valve that regulates the flow from the cold tank to the hot tank. It is clear that the TES fluid flow rate that flows through the IHX hydraulic circuit is not constant, but it is a function of the steam flow rate diverted from the BOP. All other variables including IHX pressure, tank levels, inner loop mass flow rate, and heat transfer across the IHX

are determined from the mass, energy, and momentum balances on the system. Pressure relief lines connect the shell side of the IHX with the condenser to prevent over-pressure scenarios during periods of low condensation rate.

The main constraint is associated to the filling of the hot tank. When it is nearly full and the system is in "charging" mode, the amount of steam diverted from the BOP needs to be decreased. Should the hot tank fill up, the storing capacity of the system is saturated, and then the pressure relief valves in the IHX will open when the stop valve between the cold tank and hot tank closes. From that moment on, all the steam that is bypassed needs to be directly disposed to the condenser. This scenario should be avoided since it represents a waste of high-quality steam, and it could lead to the degradation of a very expensive component like the condenser [9]. The RG block is meant to prevent the intervention of the safety valves during normal operation. To this aim, a dedicated constraint imposing that the level in the hot tank needs to stay below a certain percent full at all times will be set. Thanks to this safety-oriented shrinking of the normal operation envelope, the operational bounds are never reached, and the opening of the safety valves is definitely prevented.

Figure 7-3. TES configuration in "charging mode" and in "discharging mode" (Refer to [9]).

"Discharging" mode

During periods of peak demand, the system is discharged by pumping TES fluid from the hot tank to the cold tank through the tube side of a once-through steam generator (OTSG) producing a saturated liquid-vapor mixture. This saturated steam can then be reintroduced into the power conversion cycle prior to the moisture separator/reheaters before entering the low-pressure turbine. As with the TES operation in "charging mode", the main constraint to be addressed during the "discharging mode" is associated to the filling of the cold tank. If it is completely filled, then the hot fluid from the hot tank cannot be discharged any more, and the electricity production capability is run out [9].

TES scheduling parameter

During the "charging mode", the hot tank gets filled with the TES fluid that is heated up by the generated steam flow rate. The steam flow rate diverted from the BOP is a function of the electrical power output demanded to the steam turbine. In particular, if the nuclear reactor is operated as a base-load unit, the produced steam flow rate is constant, and then the fraction that is diverted to the TES depends on the BOP power level only (Figure 7-4).

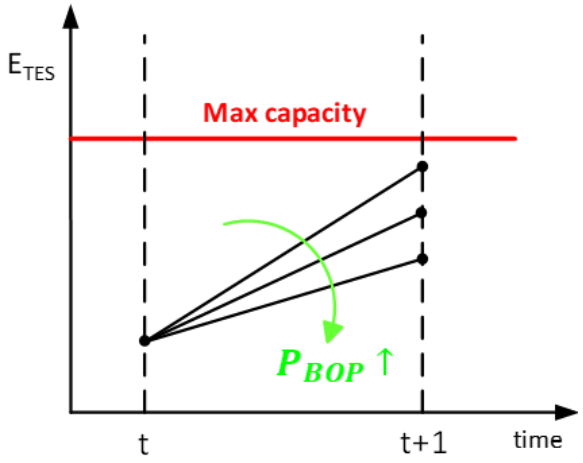

Figure 7-4. TES stored energy trajectories as function of the demanded BOP level.

To this aim, the state-space representation matrices can be parametrized with respect to the value of the incoming steam flow rate, and then to the instantaneous BOP power level. As long as the TES fluid flow rate in the circuit is a univocal function of the bypass steam flow rate, which depends on the BOP power level, the proposed parameterization holds. During the "discharging mode", the TES response is influenced by the cooling water flow rate that is flowing through the OTSG. The parametrization can then be performed with respect to the electrical power output demanded to the TES.

Table 7-1. Adopted scheduling parameters for the IES components.

IES component	Scheduling parameter	
BOP	BOP power level	
SES	SES power level	
TES	BOP power level (*charging mode*)	OTSG power level (*discharging mode*)

The parameters that were used to parametrize the LTI models are reported in Table 7-1. One issue that might complicate the proposed parametrization of the state-space representation matrices is the level of the TES fluid inside the tanks might. As abovementioned, the TES fluid level will affect the pressure, and the pressure might determine a different operating point of the pump that regulates the TES fluid flow rate. Currently, this is considered a second order phenomenon, and its impact on the TES dynamics is neglected.

8. SIMULATION OF THE POWER DISPATCH PROBLEM

As shown in Figure 2-1, a test-case composed by the three components listed in Table 7-1 was developed in HERON to assess the new role of the supervisory control in the power dispatch optimization framework. The BOP, the SES and the TES are supposed to meet the time-dependent

demand by maximizing the IES unit profitability, by respecting the power generation and energy storage capacity of each unit. As for the adopted assumptions, the electricity price is fixed ($400/MWh), as well as the power generation and the energy storing costs (Table 8-1). Note that these cost values are designed to prove the concept of parameterized supervisory control (these values do not reflect the real market trends).

Table 8-1. Adopted power generation costs and storage costs for the IES components.

IES component	Power generation cost	Energy storing cost
BOP	$100/MWh	N/A
SES	$200/MWh	N/A
TES	$300/MWh	-$300/MWh

In this test case, a 24-hour sine wave-shaped market demand profile was issued to the power dispatcher, as depicted by the purple curve in Figure 8-1. Due to the low power generation costs, the BOP and the SES will tend to operate at the maximum power allowed by the implicit constraints (Figure 8-2a, b, c, d, e, f), and the surplus power generated is stored in the TES unit, as shown in Figure 8-1 and Figure 8-2g for the first 13 hours and the 24th hour. When the load demand is higher than the combined maximum power of BOP and SES, TES will discharge and output electricity, as shown in Figure 8-1 and Figure 8-2g from the 15th to the 23rd hour.

At the beginning of the 14th hour, the RG predicts that the TES will be fully charged within this hour if SES and BOP continued to generate at maximum power. This trend would lead to the violation of the implicit constraints on the status of the TES hot tank and cold tank level (Figure 8-2h, i). The RG will then limit the TES charging power to a very small value, and the SES power level was adjusted to meet the market demand as shown in Figure 8-1 and Figure 8-2d, e. Due to its lower power generation cost, the BOP continues to operate at its maximum allowed power (Figure 8-2a, b, c), and it will be the second unit to be turned down if load demand keep dropping.

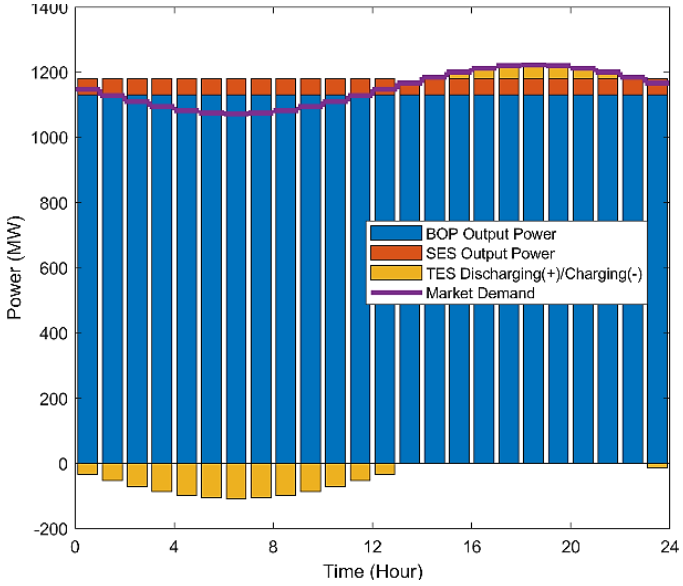

Figure 8-1. Simulation outcomes of the power dispatch problem. The BOP, SES, and TES contributions are represented.

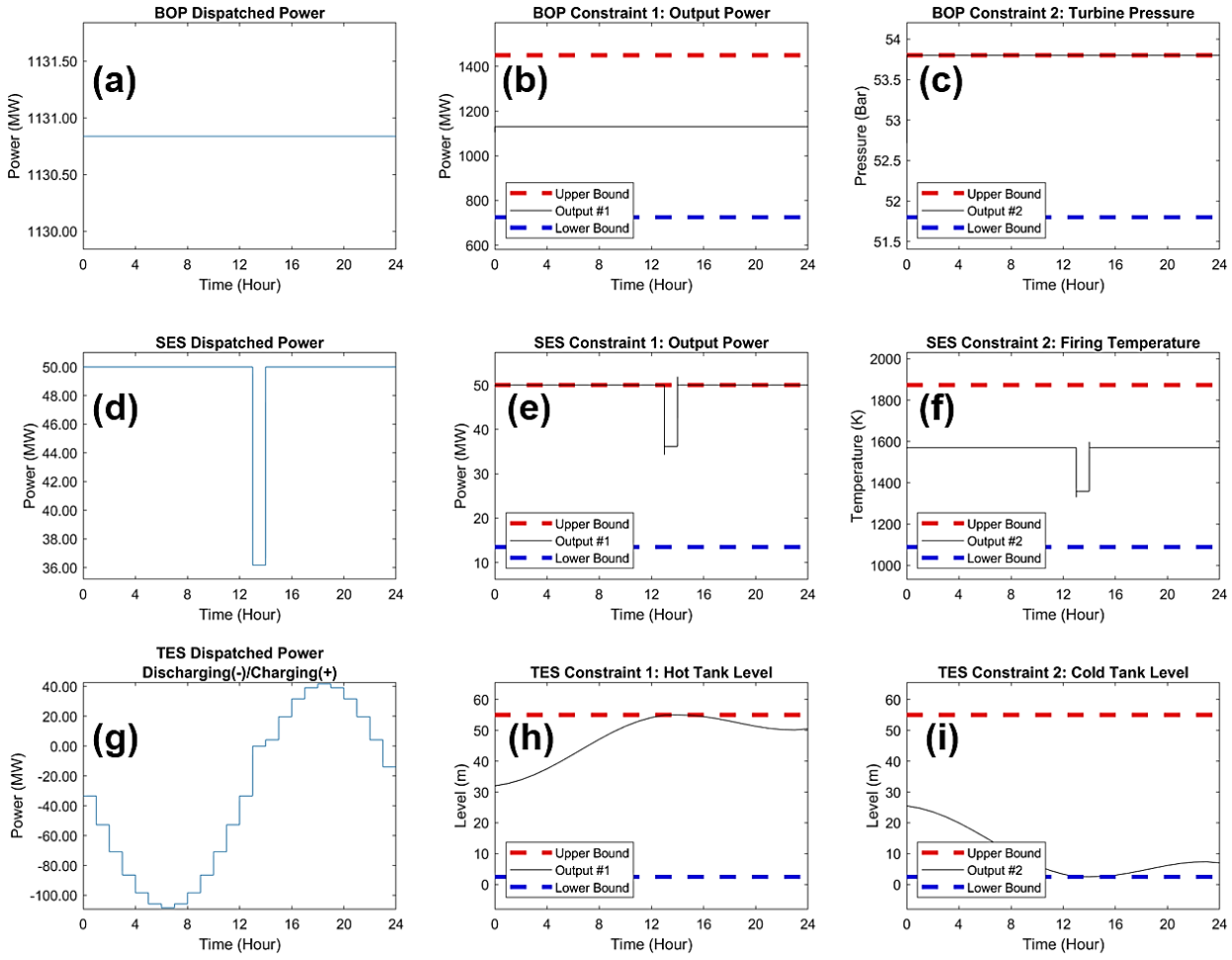

Figure 8-2. Power outputs and constrained process variable evolution of the IES components.

9. CONCLUSIONS

In this work, an RG-based algorithm to account for implicit constraints in the power dispatch optimization problem was presented. Traditionally, the RG is a scheme placed upstream to the feedback controllers that adjusts the set-point trajectories to enforce state and control constraints. The proposed configuration foresees an iterative loop between the power dispatcher and the RG that allows accounting for both the explicit and the implicit constraints. To provide the RG with the state-space representation matrices, a data-driven procedure that allows (1) reconstructing the state of the system and (2) deriving a LTI model approximation of the dynamics of the IES components at different power levels was developed. An exhaustive characterization of the system dynamics was performed off-line, and a comprehensive database of state-space representation models at different operating conditions was created. Finally, to assess the performance of the developed scheme, a representative power dispatch problem involving a three-unit system was simulated and the corresponding simulation outcomes were shown. As for the future developments, the next steps would consist in improving the accuracy of the models fed to the RG algorithm. To this aim, the integration of the state selection and the DMDc algorithms into an on-line system identification procedure would ensure a closer approximation of the dynamics of the IES components.

10. REFERENCE

[1] C. Rabiti, A. Alfonsi, J. Cogliati, D. Mandelli, R. Kinoshita, S. Sen, C. Wang, J. Chen, "RAVEN User Manual", INL/EXT-15-34123 (2016).

[2] P.W. Talbot, A. Gairola, P. Prateek, A. Alfonsi, C. Rabiti, R.D. Boardman, "HERON as a Tool for LWR Market Interaction in a Deregulated Market". INL/EXT-19-56933 (2020).

[3] H. Wang, R. Ponciroli, R.B. Vilim, A. Alfonsi, "Development of Control System Functional Capabilities within the IES Plug-and-Play Simulation Environment", ANL/NSE-20/35 (2020).

[4] A.A. Bachnas, R. Tóth, J.H.A. Ludlage, A. Mesbah, "A review on data-driven linear parameter-varying modeling approaches: A high-purity distillation column case study", Journal of Process Control, 24, 272-285 (2014).

[5] MATLAB, "Linear Parameter-Varying Models", available at www.matworks.com. Accessed on 11/29/2020.

[6] A. Casavola, F. Tedesco, E. Garone, "The distributed command governor approach in a nutshell", Distributed MPC Made Easy, Chapter 14, Springer (2013).

[7] J.L. Proctor, S.L. Brunton, J.N. Kutz, "Dynamic mode decomposition with control", SIAM Journal on Applied Dynamical Systems, 15(1), 142-161 (2016).

[8] P.J. Schmid, "Dynamic mode decomposition of numerical and experimental data", Journal of Fluid Mechanics, 656(1), 5-28 (2010).

[9] K. Frick, J.M. Doster, S. Bragg-Sitton, "Design and Operation of a Sensible Heat Peaking Unit for Small Modular Reactors," Nuclear Technology, 205, 415-441 (2019).

.

Nuclear Science and Engineering (NSE) Division
Argonne National Laboratory
9700 South Cass Avenue, Bldg. 208
Argonne, IL 60439

www.anl.gov

Argonne National Laboratory is a U.S. Department of Energy
laboratory managed by UChicago Argonne, LLC